Cell Reports
Physical Science

CellPress
OPEN ACCESS

Article

Synthetic duty cycles from real-world autonomous electric vehicle driving

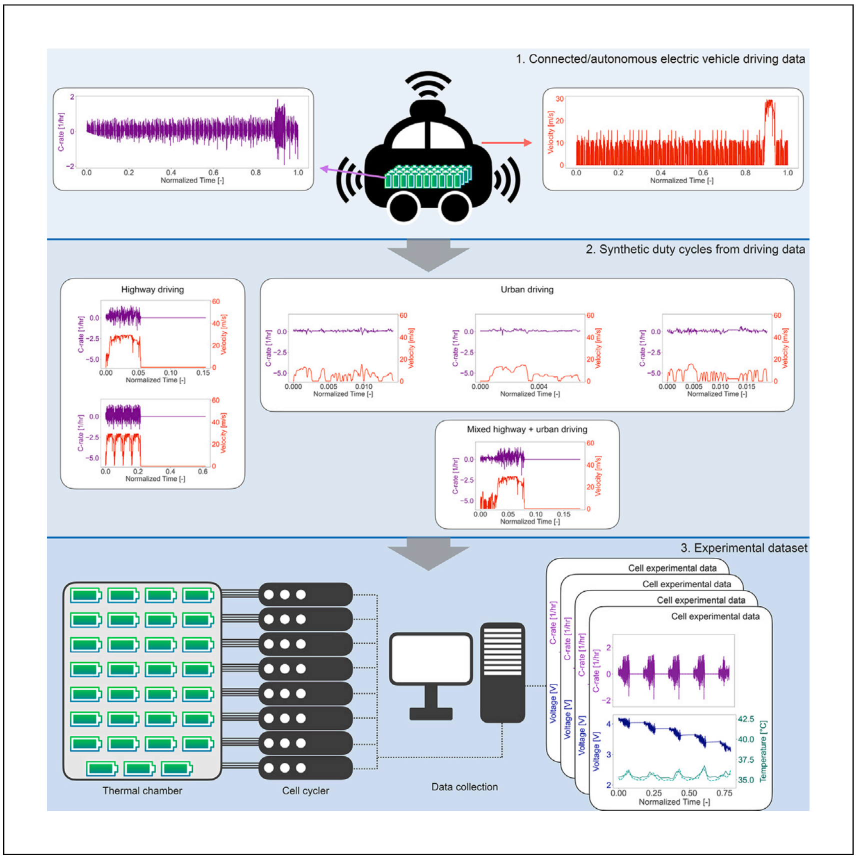

Moy et al. show that battery systems used in connected/autonomous electric vehicles undergo different usage scenarios from human-driven electric vehicles. Driving data directly from connected/autonomous electric vehicles are used to generate synthetic duty cycles, which are subsequently used to test 31 lithium-ion battery cells.

Kevin Moy, Devi Ganapathi, Alexis Geslin, William Chueh, Simona Onori

sonori@stanford.edu

Highlights

Analysis of connected/autonomous electric vehicle versus battery electric vehicle usage

Synthetic-duty-cycle generation comes directly from connected/autonomous vehicle data

Experimental design spans multiple use cases and battery system sizes

Dataset of 31 lithium-ion battery cells represents connected/autonomous vehicle usage

Moy et al., Cell Reports Physical Science 4, 101536
August 16, 2023 © 2023 The Author(s).
https://doi.org/10.1016/j.xcrp.2023.101536

Please cite this article in press as: Moy et al., Synthetic duty cycles from real-world autonomous electric vehicle driving, Cell Reports Physical Science (2023), https://doi.org/10.1016/j.xcrp.2023.101536

Cell Reports
Physical Science

CellPress
OPEN ACCESS

Article

Synthetic duty cycles from real-world autonomous electric vehicle driving

Kevin Moy,[1,3,4] Devi Ganapathi,[2,3,4] Alexis Geslin,[2,3,4] William Chueh,[2,3] and Simona Onori[1,3,5,*]

SUMMARY

Connected/autonomous electric vehicles (C/AEVs) have the potential to provide safe, efficient, and low-carbon-emission transportation solutions. Proper and efficient management of the C/AEV lithium-ion battery (LIB) system is key to guaranteeing that all benefits associated with C/AEVs are achieved. This requires that the design and control of LIBs be informed by the C/AEV system operation. This article first demonstrates that C/AEV operation is distinct from human-driven electric vehicle operation, thus necessitating the development of application-specific testing protocols to properly characterize and model their LIBs. Laboratory-prone synthetic duty cycles are generated from C/AEV driving data, enabling a design of experiments representing a wide range of C/AEV driving modes and LIB system sizes. We share data collected from 31 LIB cells undergoing the synthetic cycling experiments. This paper provides the academic community with an application-specific C/AEV LIB dataset for the design and calibration of data-driven battery models for real-time control and operation.

INTRODUCTION

Connected/autonomous electric vehicles (C/AEVs) combine the benefits of autonomous vehicles and EVs. The Society of Automotive Engineers (SAE) defines six levels of vehicle autonomy (L0 through L5) in increasing degrees of autonomy, with L0 representing full human driver control and L5 requiring no level of human interaction or control.[1] At high levels of autonomy (L4/L5), autonomous vehicles can be networked to form fleets of CAVs, which can improve traffic conditions at wide-scale deployment. CAVs have been demonstrated in simulation to improve traffic flow stability and increase traffic throughput[2] and to reduce stop-and-go traffic patterns in favor of "smooth driving,"[3] and in field experiments, fleet-level control of CAVs dissipated stop-and-go waves that, unfettered, would propagate and cause traffic.[4] C/AEVs have different operational characteristics from human-operated EVs or individually operated AEVs. As C/AEVs are autonomously operated and fleet optimized, the overall driving characteristics (e.g., acceleration and braking) will be different from human-operated EVs.[5–7] Additionally, C/AEVs can operate for between 10 and 16 h per day, far different from the traditional single-ownership model of EV driving where the vehicle is inactive for upwards of 90% of the day.[8]

The different operation of C/AEVs compared with human-driven EVs impacts the operation of lithium-ion battery (LIB) systems in each vehicle as well. The LIB systems in C/AEVs will be continuously discharged during all-day driving to near-empty states of charge (SOCs) and then will be charged with a predefined protocol to then be discharged fully the next day. In other words, in C/AEVs, the LIB system is fully discharged and charged in a consistent manner every day. In contrast,

[1]Department of Energy Resources Engineering, Stanford University, 367 Panama Street, Stanford, CA 94305, USA

[2]Department of Materials Science and Engineering, Stanford University, 496 Lomita Mall, Stanford, CA 94305, USA

[3]Applied Energy Division, SLAC National Accelerator Laboratory, Menlo Park, CA 94025, USA

[4]These authors contributed equally

[5]Lead contact

*Correspondence: sonori@stanford.edu

https://doi.org/10.1016/j.xcrp.2023.101536

This is an open access article under the CC BY-NC-ND license (http://creativecommons.org/licenses/by-nc-nd/4.0/).

human-driven EVs often only experience two trips per day (e.g., from home to work and back), therefore sitting idle for the majority of the day, and often spend multiple days before being charged again.[9] Furthermore, human-driven EVs exhibit a broad range of minimum SOCs before charging, with approximately half of charging events starting above 50% SOC.[10,11] Together, this means that the depth of discharge is much less severe, and the average SOC much higher, than for LIB systems in C/AEVs. The different operating characteristics of C/AEVs versus human-driven EVs will have different impacts on their respective LIB systems for both real-time operation as well as long-term degradation, as these impacts are highly dependent on the application-specific cycling induced on the LIBs. These impacts must therefore be studied rigorously, necessitating the development of C/AEV-specific duty cycles to replicate this application fully on LIB cells in a laboratory setting.

Duty cycles are used in laboratory experiments to generate application-specific battery data. A duty cycle is a control signal representing a response to operation in a particular application. In the context of this article, a duty cycle is a power or current profile representing the LIB cell dispatch (charge and discharge). In the simplest case, duty cycles can be constant-current/constant-voltage (CCCV) charge and discharge cycles, but duty cycles for individual EVs presented in the literature have predominantly leveraged existing drive cycles developed for testing internal combustion engine (ICE) vehicles, including DST and FUDS,[12] UDDS and US06,[13] ARTEMIS,[14] and NEDC.[15] These drive cycles are reported as vehicle velocity as a function of time, as they are intended for vehicle dynamometer testing. In order to produce current input signals for duty cycling, external tools such as ADVISOR[16] or other vehicle simulators[17] are used to model the EV drivetrain and extract the voltage and current output of the LIB pack. This must then be scaled down to the cell or the module level for laboratory testing. Few studies in the literature develop and apply duty cycles generated directly from driving data, instead of from existing drive cycles. For example, vehicle velocity data from three different trips were used to compare the responses between LIB systems simulated for different EV models by Sun et al., but these trips were selected *ad hoc* and were not further synthesized into duty cycles.[18] Drive cycles were synthesized directly from EV trip data by Gong et al.,[19] and ARTEMIS drive cycles were modified by Duan et al. to account for different objectives for autonomous EV driving characteristics (e.g., smooth versus "swift" driving),[5] but neither study converted these drive cycles into duty cycles, nor did they apply them in laboratory LIB experiments.

Additionally, these studies still do not explicitly model the C/AEV use case where the vehicles are continuously driven in charge-depleting mode through their entire operating range until the LIB system minimum SOC is reached. As LIBs exhibit substantial differences in response between those cycled with arbitrarily selected synthetic duty cycles compared with those cycled with duty cycles collected from real driving data,[19,20] laboratory study of C/AEV LIB systems must use application-specific duty cycles, as has been previously done for human-driven hybrid EVs and EVs.

To this end, this article presents the following contributions.

(1) A quantitative comparison demonstrating that C/AEVs yield operational characteristics distinct from those in human-driven EVs, which in turn imposes different operational characteristics of their respective LIB systems.
(2) The development of six synthetic duty cycles from LIB cell current and vehicle velocity data representing real-world C/AEV operation in two different cities,

Cell Reports
Physical Science
Article

CellPress
OPEN ACCESS

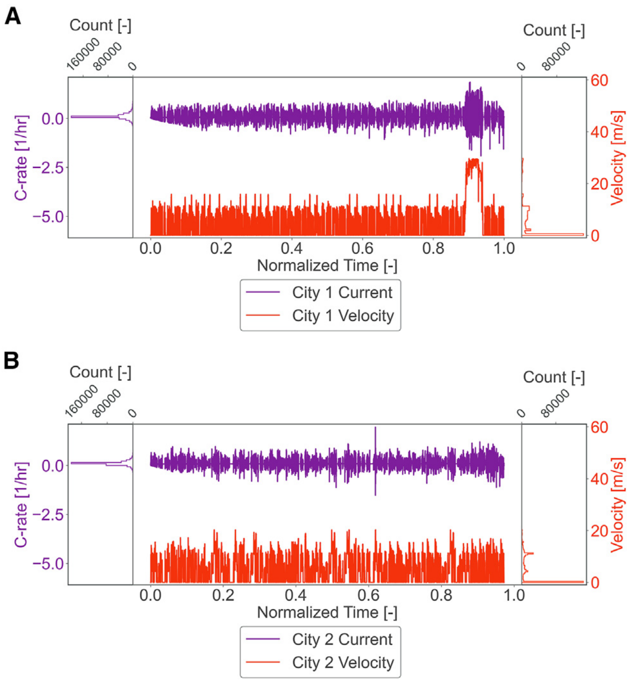

Figure 1. C/AEV driving datasets

C/AEV driving datasets (CDDs) are plotted for (A) City 1 and (B) City 2, with histograms on either side for the cell current (left) and vehicle velocity (right) distributions. The x axes of both plots are normalized to the city 1 CDD duration.

used to design a suite of protocols representing a wide range of operating modes for C/AEV LIB systems.

(3) A comprehensive experimental dataset collected from a batch of 31 high-nickel-content LIB cells cycled with these synthetic-duty-cycle-based protocols, made available to the academic community.

Broadly speaking, the synthetic-duty-cycle approach in this article and its resulting dataset will help guide proper design of C/AEV LIB systems, inform real-time C/AEV-specific control and management of LIB systems, and enable machine-learning approaches for remaining useful life and end-of-life prediction.

RESULTS AND DISCUSSION

C/AEV driving datasets

The C/AEV driving datasets (CDDs) in this article consist of vehicle velocity data collected from real-world autonomous hybrid EV driving in two cities (City 1 and City 2), spanning both urban (intra-city) driving and highway driving, in units of meters per second. The vehicle velocity was used in simulation to produce the current for one cell in a C/AEV LIB system in units of C-rate (current in amperes normalized to cell capacity in ampere hours). The CDDs presented in this study represent one full day of C/AEV operation under the assumption that the C/AEV is charged fully and only overnight and then discharged throughout the day during vehicle driving. All data are obtained as time-series data sampled at 0.1 s resolution. Positive current corresponds to discharge, and negative current corresponds to charge. Figure 1 shows the CDDs used in this article. For direct comparison between figures, the x axes for all time-series figures in this article are normalized to the longer of the two datasets (city 1).

Table 1. Summary of interval metrics as applied to micro-trips

Number	Name	Unit
1	peak discharge C-rate	1/h
2	peak charge C-rate	1/h
3	average discharge C-rate	1/h
4	average charge C-rate	1/h
5	variance of discharge C-rate	$1/h^2$
6	variance of charge C-rate	$1/h^2$
7	average total C-rate	1/h
8	peak frequency in discharge	Hz
9	peak frequency in charge	Hz
10	distance traveled	m
11	peak velocity	m/s
12	average velocity	m/s
13	variance of velocity	m^2/ s^2
14	number of starts from zero velocity	unitless

These metrics are used in the synthetic-duty-cycle algorithm (Algorithm 1 in Note S1), as well as in comparing C/AEV driving with human-driven EV driving. A complete description of each of these metrics is in Note S1.

Comparison of CDDs with human-driven EV driving data

The 14 metrics in Table 1 are used to compare the operational characteristics of the City 1 and City 2 CDDs with those of a driving dataset from a human-driven EV in the Vehicle Energy Dataset (VED), which presents data such as velocity, current, and SOC as recorded from real-world driving.[21] Each dataset is segmented into "micro-trips," defined as periods of active driving between idle (zero-velocity) periods no less than 30 s in length; this process is summarized in Figure S1. The metrics in Table 1 are then computed for each of the micro-trips within the dataset. These results are summarized as boxplots in Figure 2, allowing for direct comparison of the distribution of metric values for micro-trips as computed for the C/AEV and human-driven EV datasets. For example, the average velocity of the human-driven EV is up to twice that observed in the CDDs. Furthermore, while the minimum recorded SOC from the human-driven EV was 21%, its SOC largely remained above 50%, demonstrating the smaller SOC range of human-driven EVs compared with C/AEVs. Altogether, this demonstrates the distinct differences between LIBs operating in C/AEVs versus human-driven EVs and therefore necessitates the synthesis of application-specific C/AEV duty cycles for laboratory testing.

Synthetic duty cycles

The synthesis of duty cycles from existing datasets has previously been applied for generic vehicle driving (i.e., without considering the propulsion method),[22] hybrid EVs,[23] EVs,[20,24–26] and grid-scale energy storage[27–29]; the method presented in this article modifies the authors' previous work on synthetic duty cycles.

Six synthetic duty cycles were obtained from the City 1 and City 2 CDDs, described in Table 2. These consist of one urban-driving synthetic duty cycle for each city (2a, 2b); one urban-driving synthetic duty cycle that combined urban driving from both cities (2c); two highway-driving synthetic duty cycles (1a, 1b); and one synthetic duty cycle that combines both urban and highway driving from both cities (3). These synthetic duty cycles all have an average C-rate of C/10, representing a full 10 h day of C/AEV driving. Figure 3 shows all six synthetic duty cycles and a comprehensive visual representation of their relationship to the City 1 and City 2 CDDs. For more detailed information on duty-cycle synthesis, the reader is referred to Note S1; a summary of the generation process follows below.

Cell Reports
Physical Science
Article

CellPress
OPEN ACCESS

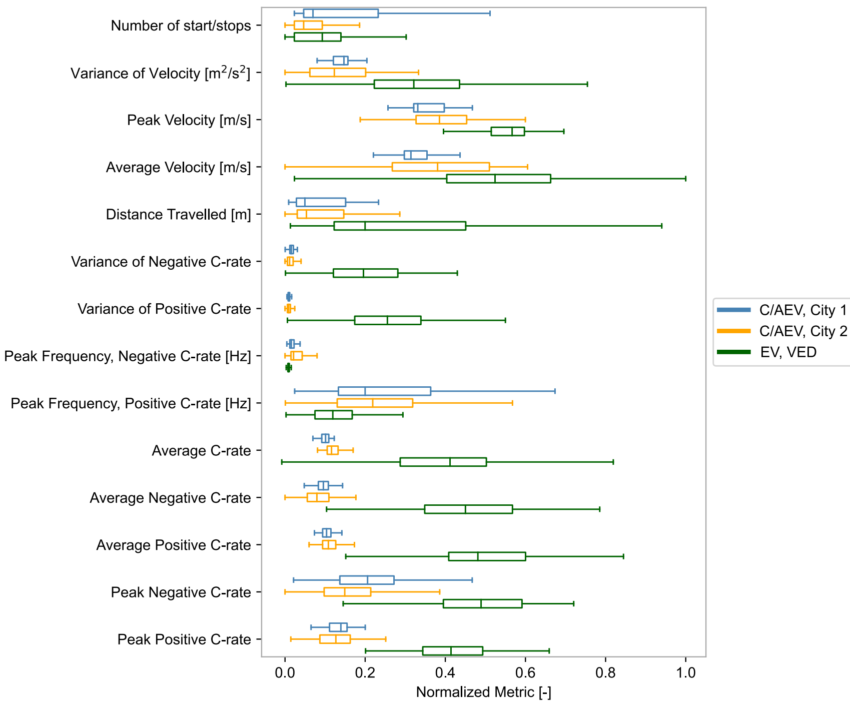

Figure 2. Boxplots showing metrics in Table 1 as calculated for the City 1 (blue) and City 2 (orange) CDDs shown in Figure 1, as well as data collected from a human-driven EV (green) in the Vehicle Energy Dataset (VED)

For each boxplot, the box extends from the first quartile to the third quartile of the corresponding data, with a line at the median of the data. The whiskers extend from the box by 1.5 times the interquartile range. The x axis is normalized to the maximum value for each metric.

For urban driving, the synthetic-duty-cycle algorithm (Algorithm 1 in Note S1) was developed, based on previous work from the authors.[30] The algorithm takes a CDD as its input and segments it into “micro-trips” as previously defined. A matrix is formed by computing metrics corresponding to different features of C/AEV driving for each micro-trip; these metrics are summarized in Table 1. This forms a matrix with dimensions corresponding to the number of micro-trips and the number of metrics, respectively: 104 × 14 for the city 1 CDD, 142 × 14 for the city 2 CDD, and 245 × 14 for the combined city 1 and city 2 CDD. Principal-component analysis is used to reduce the dimensionality of each matrix to 104 × 6 for the city 1 CDD, 142 × 6 for the city 2 CDD, and 245 × 7 for the combined city 1 and city 2 CDD, respectively. *k*-means clustering is applied to the rows of each reduced-dimension matrix to identify characteristic micro-trips within each corresponding CDD, and these are then concatenated to form the synthetic duty cycle, which is then returned by the algorithm. In order to accommodate the experimental hardware and data collection pipeline, the duty cycles are then downsampled from the original 0.1 s resolution to a 1 s resolution.

It is worth noting that the SOC and the voltage from the CDDs were not used to compute any metrics, in contrast to Moy et al.,[30] where the state of energy of the grid storage pack was used. This is due to a key difference between the C/AEV and grid storage dispatch data. The CDDs correspond to charge-depleting behavior, where the LIB ends at a lower SOC than at which it started. In addition, as the LIB SOC decreases, so does its voltage. Then, the SOC and voltage values are within distinct ranges for each micro-trip, and the corresponding computed

Please cite this article in press as: Moy et al., Synthetic duty cycles from real-world autonomous electric vehicle driving, Cell Reports Physical Science (2023), https://doi.org/10.1016/j.xcrp.2023.101536

Table 2. Description of each synthetic duty cycle generated in this work, as well as the combinations of synthetic duty cycle and average C-rate included in the experimental dataset

		Average C-rate			
Synthetic duty cycle	Description	C/16	C/10	C/5	C/2
1a	single highway micro-trip (city 1) with rest determined as in Note S1	I, II	I, II	I, II	–
1b	four consecutive highway micro-trips (city 1) with rest determined as in Note S1	I, II	I, II	–	–
2a	synthesized from urban driving in city 1	–	I, II	I, II	I, II
2b	synthesized from urban driving in city 2	–	I, II	I, II	I, II
2c	synthesized from urban driving in both city 1 and city 2	–	I, II	II	I, II
3	mixed urban and highway driving: concatenation of 2a, 2b, 2c, and 1a	–	I, II	I, II	–

The Roman numerals (I, II) within each entry denote the cell duplicates. Details on this selection of combinations can be found in the experimental procedures. Experimental data corresponding to the column for average C-rate of C/10 are plotted in Figure 4. The cell corresponding to synthetic duty cycle 2c at an average C-rate of C/5 duplicate I shorted at the beginning of the experiment, and so the corresponding data are unavailable in the dataset.

metrics (e.g., average SOC during discharge) are also distinct for each micro-trip and therefore do not yield any additional information for clustering and data reduction.

For highway driving, only one micro-trip across both CDDs met the highway driving criteria (average velocity $\geq$ 20 m/s), outlined and shaded in dark blue on the City 1 CDD in Figure 3. Therefore, a different method was used to form synthetic duty cycles with the same average C-rate as the urban synthetic duty cycles by adding rest periods to the highway-driving micro-trip. Synthetic duty cycle 1a cycles between a single highway-driving micro-trip and a rest period, while synthetic duty cycle 1b cycles between four consecutive highway-driving micro-trips and a rest period four times as long as that in synthetic duty cycle 1a. In both cases, the rest period length was chosen to maintain an average C-rate of C/10 to match those of the urban-driving synthetic duty cycles. As with the urban-driving synthetic duty cycles, synthetic duty cycles 1a and 1b are downsampled to 1 s resolution.

Finally, synthetic duty cycle 3 is the concatenation of synthetic duty cycles 2a, 2b, 2c, and 1a, in that order, consisting of a mix of urban-driving synthetic duty cycles obtained from three different datasets (City 1, City 2, and both City 1 and City 2 for synthetic duty cycles 2a, 2b, and 2c, respectively), as well as the single highway-driving micro-trip represented in synthetic duty cycle 1a.

The six synthetic duty cycles represent different modes of driving. The short highway driving of synthetic duty cycle 1a could represent highway driving from home to work, while the longer highway driving in synthetic duty cycle 1b could represent longer trips with longer rest periods, such as a day trip to the beach. Synthetic duty cycles 2a and 2b could represent driving only within City 1 and City 2, respectively, whereas synthetic duty cycle 2c could represent a vehicle used for driving within both City 1 and City 2 metropolitan areas. Finally, synthetic duty cycle 3 includes driving between different cities with different road conditions as well as highway driving, representing vehicles that experience a variety of driving conditions. Figure S2 shows the wide range of operating characteristics, as defined by the metrics in Table 1, represented across the six synthetic duty cycles. Notably, the synthetic duty cycles maintain the same average C-rate, which is key to developing the full range of the experimental dataset in the following section.

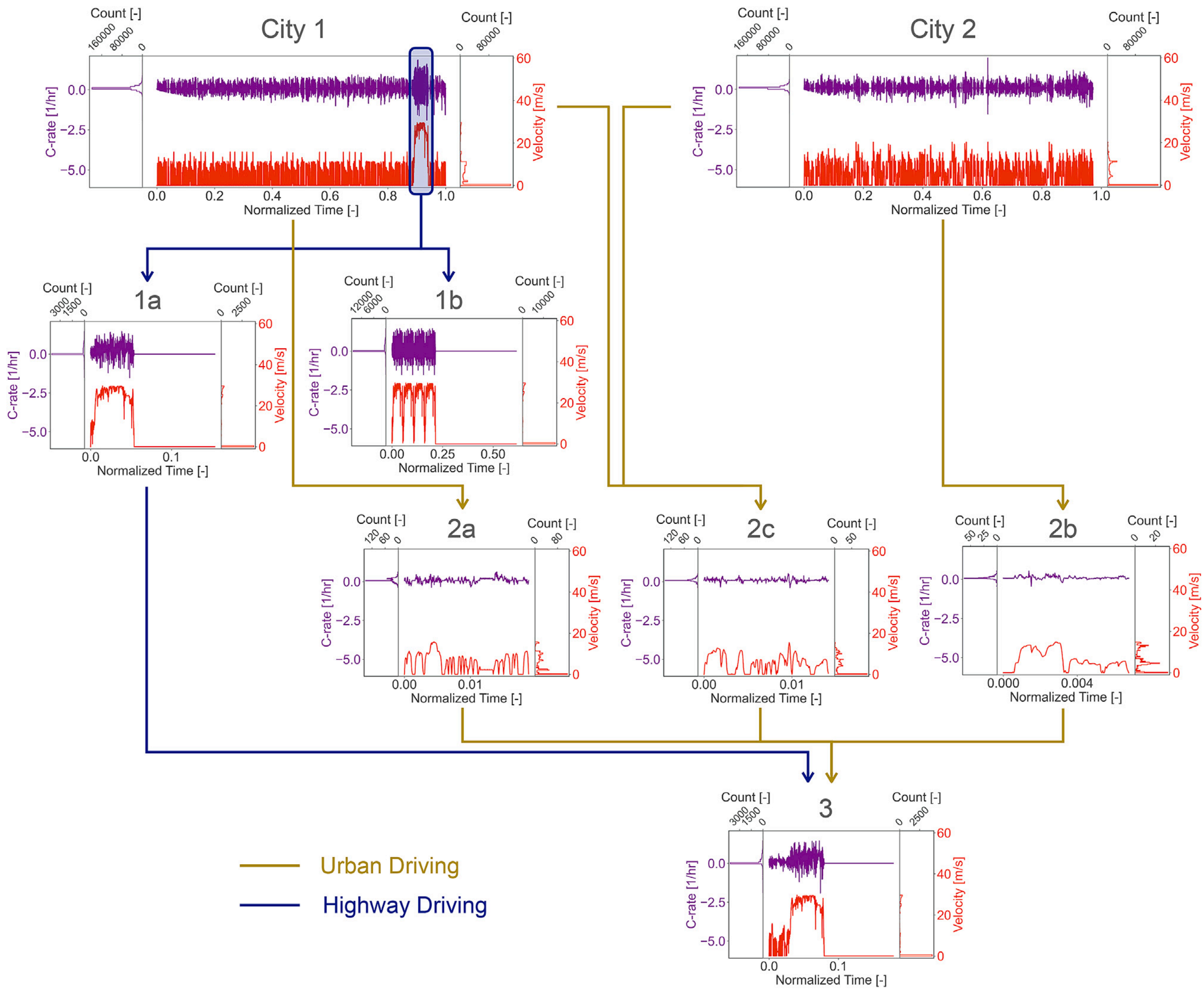

Figure 3. Overview of the relationship between the city CDDs and the synthetic duty cycles presented in this article

At top, the current and velocity data from the city 1 and city 2 CDDs shown in Figure 1 are used to generate the synthetic duty cycles. The highway-driving micro-trip in city 1 is highlighted and boxed in blue, and its resulting synthetic duty cycles are connected via blue arrows. The relationship between the city CDDs and the resulting urban-driving synthetic duty cycles are shown using dark gold arrows. Synthetic duty cycle 3 is the concatenation of synthetic duty cycles 2a, 2b, 2c, and 1a and therefore contains a combination of both urban as well as highway driving. As with the city CDDs, each synthetic duty cycle is plotted with histograms on either side for the cell current (left) and vehicle velocity (right) distributions. The x axes of all plots are normalized to the city 1 CDD duration.

Experimental dataset

The dataset presented in this article comprises experimental data collected from a batch of 31 identical high-nickel-content LIB cells (please see the data and code availability section for more information). Figure S4 summarizes the process from synthetic-duty-cycle generation to collection of experimental data. Each protocol (i.e., combination of synthetic duty cycle and average current) is conducted in duplicate on two cells, both for experimental redundancy as well as the study of variation in battery response to identical duty cycling (as in the discussion). The experiments take place in a thermal chamber with a temperature setpoint of 35°C, where all cells are cycled from a maximum voltage of $V_{max} = 4.2$ V to a minimum voltage of $V_{min} = 3.1$ V following battery specifications. A subset of this dataset from all cells cycled at average C-rate C/10 is shown in Figure 4.

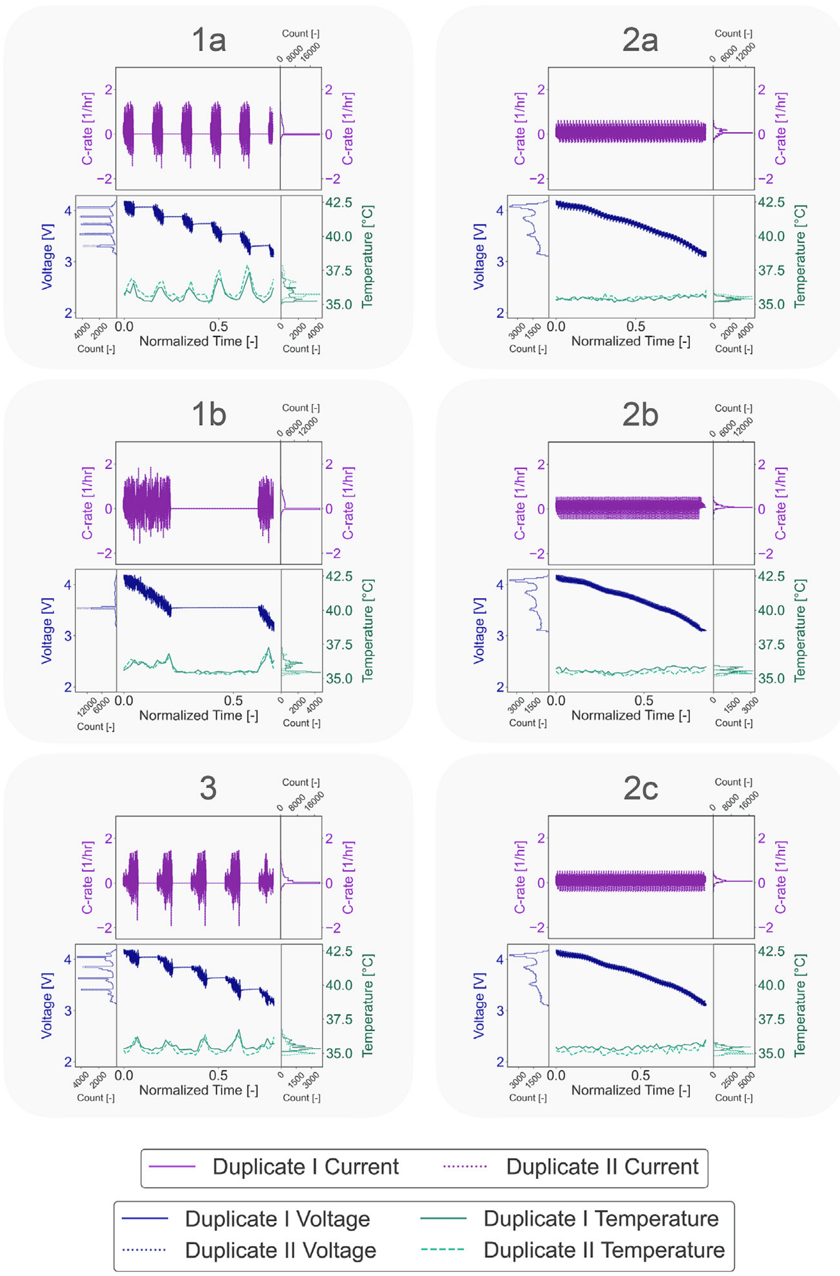

Figure 4. Experimental data generated by this study for an average C-rate of C/10, labeled by the six synthetic duty cycles, and plotted for each set of cell duplicates for each duty cycle
For each synthetic duty cycle, the top subplot shows the synthetic-duty-cycle current profiles for each cell duplicate, plotted with the corresponding histograms of measured cell current on the right of each plot. Positive current corresponds to discharge. The bottom subplot contains the voltage (blue) and temperature (green) responses from the input current profiles for each duplicate, with histograms on either side of the plot for the measured voltage (left) and temperature (right) values. The x axes in all plots are normalized to the city 1 CDD duration.

Since the synthetic duty cycles are all generated with the same average C-rate, they can all be scaled to create duty cycles of various different average C-rates. This allows for an experimental design that induces a wide range of different operating conditions that could be experienced by C/AEV LIBs. As an example, consider as

Cell Reports
Physical Science
Article

CellPress
OPEN ACCESS

a baseline case a cell cycled with the City 1 urban-driving synthetic duty cycle 2b at an average current of C/10 (shown in Figure 3, third row from top at right, with experimental data in Figure 4 at middle right). Increasing this current to a C/2 average current (experimental data shown in Figure S7) could be interpreted as an LIB pack with cells of smaller capacity driving the same vehicle; these cells must increase their output current in order to produce the same pack power output as the baseline case. Changing the synthetic duty cycle to the highway-driving synthetic-duty-cycle synthetic duty cycle 1a (shown in Figure 3, second row from top at left, with experimental data in Figure 4 at top left) while maintaining the same average current simulates the same LIB pack used for a C/AEV used primarily on the highway instead of in urban environments.

To this end, the protocols included in the experimental dataset span several different average C-rates for each of the six synthetic duty cycles, simulating fleet operation of C/AEVs driving under different conditions. Along with the descriptions of each synthetic duty cycle, Table 2 summarizes all protocols for all cells in the dataset and is also used to construct the reference labels for each cell in the dataset. For example, reference label "1a (C/16) - I" is the first cell duplicate cycled with synthetic duty cycle 1a at an average C-rate of C/16.

Synthetic-duty-cycle response behavior

Figure 4 provides a way to analyze the voltage and temperature responses of LIB cells by the synthetic duty cycle inputs. For example, in synthetic duty cycles 1a, 1b, and 3, cell temperatures increase during regions of high-current discharge and decrease and relax during the rest periods. As seen in the voltage response histograms, the voltage distributions for all synthetic duty cycles all contain distinct peaks. Data are collected in increments of time (as opposed to increments of voltage), so a plateau at a given voltage results in more data collected at that voltage, leading to a corresponding peak in the voltage distribution. However, these peaks originate from different phenomena within different duty cycles. Synthetic duty cycles 1a, 1b, and 3 contain cycling based on highway driving, which includes extended rest periods to maintain the same average C-rate as the other synthetic duty cycles. The voltage distributions for these synthetic duty cycles are dominated by the peaks resulting from these zero-current/constant-voltage periods.

In contrast, synthetic duty cycles 2a, 2b, and 2c are based on urban driving and have no extended rest periods. In the voltage distributions for these synthetic duty cycles, three main peaks are seen at approximately 4.1, 3.8, and 3.5 V. These peaks correspond to the plateaus in the voltage profiles, which are caused by the phase transitions from the graphite in the negative electrode.[31] It is interesting to note that despite the dynamic discharge behavior of these protocols, the phase transitions are still apparent in the voltage profiles as plateaus; this can be seen in Figure S6, which shows the voltage profile of a cell cycled with a constant current discharge at C/10. In other words, as far as the voltage response is concerned, these duty cycles can also be thought of as transient signals superimposed on a C/10 constant current discharge.

The experimental dataset provides a rich and diverse set of synthetic duty-cycle current inputs, as well as voltage and temperature outputs. The voltage and temperature histograms for all cells in the dataset are shown in Figure S8, demonstrating the broad range of voltage and temperatures exhibited throughout the dataset. In particular, higher average C-rates led to a shift of the temperature

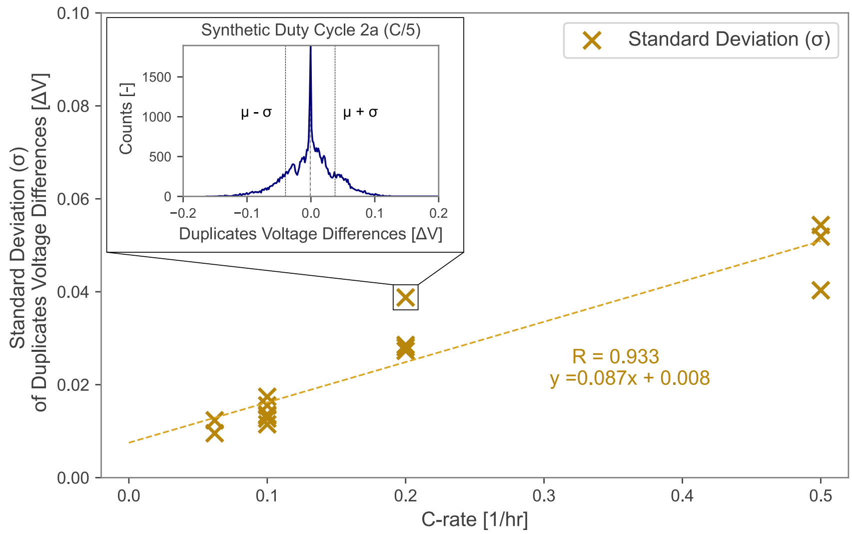

Figure 5. Standard deviation of voltage response differences between cell duplicates

The inset in the figure represents the distribution in voltage differences between duplicates for the synthetic duty cycle 2a at an average C-rate of C/5, with mean $\mu = 0$ and standard deviation $\sigma = 0.04$. The standard deviation σ of such distributions is computed for each protocol (e.g., combination of duty cycle and average C-rate) and is shown in the main plot as a function of C-rate.

distributions to higher temperatures, as can be seen by the horizontal shift in histograms moving down the right column in Figure S8. Since the reported C-rate is an average, current extrema in these duty cycles are exacerbated at higher average C-rates, leading to higher average temperatures. This can be seen by comparing the current and temperature data for synthetic duty cycle 2b at average C-rate of C/10 (in Figure 4, middle row at right), with data from a cell cycled with the same duty cycle but at an average C-rate of C/2 (in Figure S7).

Voltage response differences between cell duplicates

From the duplicates in the dataset, the consistency of the voltage response to the same applied current stimulus is also investigated. For a given protocol, the differences between the voltage curves of the two duplicates are calculated at each point and referred to as "Duplicates Voltage Differences." The inset in Figure 5 shows the distribution of these differences for synthetic duty cycle 2a (C/5) as an example. The standard deviation of the distribution of these differences can be used as a metric to quantify reproducibility of cell response to protocols across multiple cells; a low standard deviation means that the differences between duplicates with the same protocol are minimal and indicates that this protocol is reproducible across multiple cells. Figure 5 shows that the standard deviation of the duplicate voltage differences is highly correlated with the cycling C-rate (Pearson correlation coefficient $R = 0.93$). Practically, this means that a higher average C-rate will generate less reproducible voltage responses across cells cycled identically, suggesting that this arises from variations in cell resistance. A similar analysis was carried out on cell temperature responses (Note S2; Figure S3). In general, the temperature difference distributions follow a similar trend: as the C-rate increases, the spread in temperature differences between duplicates increases. This finding suggests that more sample repeats should be considered when designing C/AEV experiments involving higher C-rates in order to better capture cell-to-cell variability.

Please cite this article in press as: Moy et al., Synthetic duty cycles from real-world autonomous electric vehicle driving, Cell Reports Physical Science (2023), https://doi.org/10.1016/j.xcrp.2023.101536

Outlooks and future work

This article provides a dataset from experiments, which directly leverage C/AEV LIB cell and vehicle driving data, by cycling cells with protocols corresponding to a wide range of possible C/AEV operations. This dataset can have immediate impacts for on-board C/AEV LIB battery management systems (BMSs). These BMSs employ models that must be calibrated from battery current input and voltage/temperature response data, which accurately represent the C/AEV use case, to ensure safe real-time control of the LIB system. Using the experimental dataset in this article for BMS model development will result in C/AEV BMSs suited for the full range of battery excitation modes induced on the LIBs by the C/AEV operation represented in the dataset.

The synthetic duty cycles generated in this article will be key for investigating effects of application-specific duty cycling on aging in a laboratory environment. The cells in this article are currently being continually cycled until they reach end-of-life conditions. As the degradation trajectory of LIBs is highly dependent on the application, the aging data collected during these ongoing experiments will be useful in developing models for C/AEV LIB systems. This represents a fundamental step in understanding the differences in aging trajectories under different use cases within the C/AEV application. For example, if the cells experience a similar but less severe aging trajectory compared with those in EVs, BMSs developed for safe, aging-aware operation of EV LIB systems could be adapted for the milder C/AEV operation. On the other hand, if the C/AEV LIB aging trajectories are completely distinct from those in EV LIBs, further study is needed to develop aging-aware safety systems for C/AEV BMSs. One application of this aging data is in data-driven machine-learning models that predict the remaining useful life and end-of-life conditions for C/AEV LIB systems, which is important for determining warranties in this specific application.[32] Such models will require aging trajectories that cover a wide range of C/AEV operation, parameterized by features characterizing this operation. The cells aged with the protocols in this article, with features such as the metrics in Table 1, could provide a rich and diverse set of training data for machine learning.

The breadth of C/AEV driving captured by the synthetic duty cycles generated using the methodology in this article can be improved in future work by broadening the scope of the input data and experimental design. In this article, the CDDs comprise C/AEV driving in two different cities, and the experiments are conducted at a single temperature (35°C) on a single LIB chemistry and form factor. More combinations of characteristic micro-trips (e.g., synthetic duty cycle 3) and blends of driving datasets (e.g., synthetic duty cycle 2c) could also be used to form more comprehensive testing protocols that represent more modes of C/AEV operation. Future data collection in C/AEVs could include LIB system temperature, which could be used to incorporate usage-dependent temperature variations (and their resulting impacts on aging) during cycling.

Future work could also include an experimental design with additional cell chemistries, such as nickel-/cobalt-free chemistries, in order to inform selections in cell chemistry for the C/AEV application. The synthetic duty cycles could be used to design experiments that accelerate aging based on scaling C-rates and elevating temperatures as presented in this article. Such experiments could be used for qualification testing of LIB cells for C/AEVs. For example, if cells aged in these experiments are able to generalize the aging trajectory of C/AEV LIB systems, then the resulting aging data could be used to quickly screen different LIB cell chemistries for this application.

The synthesis and design of experiments in this article were based on duty cycling at the cell level. However, even with near-identical initial states, individual cells cycled identically can still have different voltage responses, as shown in Figure 5. This ultimately will lead to heterogeneity within the LIB system, as the cells age along different trajectories.[33] Future work could also leverage this dataset to inform a new design of experiments for heterogeneously aged cells or experiments that simulate LIB modules or packs within a C/AEV using module- or pack-level synthetic duty cycles.

The methodology presented in this article generates synthetic duty cycles from CDDs that include vehicle velocity and cell current. Generally, the synthetic-duty-cycle algorithm can accept any transient time-series data from system operation without any particular constraint on the particular application or even the energy storage technology. This algorithm is general enough to be applied to other emerging electrified transportation technologies, for example, electric vertical take-off and landing (eVTOL) aircraft, which is expected to be a $17.7 billion market in the United States alone.[34] As with C/AEVs, eVTOL applications induce different stresses on the energy storage system, including higher C-rates, higher yearly energy throughputs, and longer sustained peak-power periods, when compared with EVs.[35] Similar to the work presented in this article, real-world eVTOL data can be leveraged to create laboratory-compatible synthetic duty cycles that will inform the selection of energy storage technologies and the system-level design and control of the energy storage system for this application.

EXPERIMENTAL PROCEDURES

Resource availability

Lead contact

Further information and requests should be directed to and will be fulfilled by Simona Onori (sonori@stanford.edu).

Materials availability

This study did not generate new materials.

Data and code availability

The experimental data have been deposited at the Stanford Digital Repository under https://doi.org/10.25740/ky011nj6376 and are publicly available as of the date of publication.

All original code has been deposited at Zenodo under https://doi.org/10.5281/zenodo.8111921 and is publicly available as of the date of publication.

Experimental hardware and data acquisition

The experiments were carried out at the SLAC Battery Informatics Laboratory. The cells were cycled on a Maccor Series 4000 cycler. The temperature-controlled chamber (CSZ model #ZPS-16-2-H/AC) includes 96 channels with 10 ms standard time resolution, with all experiments conducted with a temperature setpoint of 35°C. The Maccor software MacTest32 was used to cycle the cells and acquire the data. The acquisition rate was set to 1 s.

Please cite this article in press as: Moy et al., Synthetic duty cycles from real-world autonomous electric vehicle driving, Cell Reports Physical Science (2023), https://doi.org/10.1016/j.xcrp.2023.101536

In order to monitor self-heating and/or potential thermal runaway of individual cells, the cell temperatures were monitored individually. For this purpose, individual thermocouples (OMEGA SA1-T-120) were positioned on each cell using the included self-adhesive tape. The data from the thermocouples were acquired via a DAQ system (OMEGA OM-240 24-Channel Ethernet Data Logger with Embedded Web Server). Thermocouple wires were routed out of the temperature-controlled CSZ chamber via a side port on the chamber, filled with a polymeric/foam seal, and connected to the DAQ system outside the chamber. Additional multiplexer boards (OMEGA OM-240-MUX) were daisy chained to add more thermocouple channels in series, allowing for the external temperature of each individual cell to be monitored. Temperature data from each thermocouple channel were collected approximately every 12 min (low data-collection frequency was mainly due to throughput limitations from the multiplexers).

The Maccor raw data were automatically converted to ASCII-formatted files through the ''Maccor Information Management Software'' (MIMS) Server. Along with the temperature measurements, these raw data and ASCII data files were then pushed to an Amazon AWS S3 bucket. Data analysis was carried out on the ASCII data files in an Amazon Sagemaker notebook instance using Python Jupyter Notebooks. Figure S5 shows the data generation and collection pipeline.

Synthetic-duty-cycle implementation

The synthetic duty cycles were implemented using the experimental setup as follows. Each cell was cycled with one of the combinations of average C-rate and synthetic duty cycles in Table 2. The synthetic duty cycles were downsampled to 1 s resolution due to hardware limitations, resulting in some high-frequency information loss and in the lowering of peak and average C-rates. Each particular combination of synthetic duty cycle and average C-rate was cycled on two cells to provide redundancy and robustness in anticipation of experimental failures. The experimental dataset includes discharge data from each of these cells, for which the cells start from V_{max}. The cycling protocol repeated the synthetic duty cycle in a loop for a specified number of times, calculated by dividing the inverse of the average C-rate (e.g., 10 h for a C/10 average profile) by the duration of the synthetic duty cycle. The synthetic duty cycle itself was called as a waveform in the Maccor software and had the end condition of stopping when the cell voltage reached V_{min}. The discharge protocol was programmed to loop over the synthetic duty cycle a few more times than necessary to ensure that all cells reached V_{min} by the end of each discharge cycle. After each discharge cycle, all cells were charged from V_{min} back to V_{max} with a standardized charging protocol (CCCV charge at C/2 with cutoff current of C/20).

The originally planned experiments included all six synthetic duty cycles each at average C-rate C/10, C/5, and C/2, which would have yielded a total of 48 cells. However, the synthetic duty cycles from the highway portions at C/2 average current frequently violated the upper current limit on the Maccor cyclers, so synthetic duty cycles 1a and 1b (C/2 average) were excluded. They were replaced by synthetic duty cycles 1a and 1b at a C/16 average current. Synthetic duty cycle 3 (C/2 average) was also excluded for the same reason. The 1b C/5 average current profile did not complete a full repetition of the synthetic duty cycle before reaching the lower voltage cutoff, so this protocol was also excluded from the experiments. One of the cells shorted before any data could be collected, leaving only one duplicate of synthetic duty cycle 2c at a C/5 average current. This yields the total of 31 cells described in Table 2. Finally, some synthetic duty cycles were modified to leave a buffer below the Maccor cycler limit. The protocols that were modified using this procedure were the synthetic duty cycles 1a (C/5 average), 1b (C/5 average), 2a (C/2 average), and 3 (C/5 average).

SUPPLEMENTAL INFORMATION

Supplemental information can be found online at https://doi.org/10.1016/j.xcrp.2023.101536.

ACKNOWLEDGMENTS

This research was funded in part by the National Science Foundation Graduate Research Fellowship and the Stanford Chevron Fellowship in Energy. This research used the facilities of the SLAC Battery Informatics Lab at SLAC National Accelerator Laboratory. The authors wish to thank Mayank Malik for helping create the data architecture and Vivek Lam for his contribution to the experimental work.

AUTHOR CONTRIBUTIONS

Conceptualization, K.M., W.C., and S.O.; methodology, K.M. and S.O.; software, K.M.; formal analysis, K.M., D.G., and A.G.; investigation, K.M., D.G., and A.G.; data curation, D.G.; writing – original draft, K.M.; writing – review & editing, K.M., D.G., A.G., W.C., and S.O.; visualization, K.M., D.G., and A.G.; funding acquisition, W.C. and S.O.; supervision, W.C. and S.O.

DECLARATION OF INTERESTS

D.G. is currently affiliated with Apple but was affiliated with Stanford University at the time the research was conducted.

Received: March 13, 2023
Revised: May 31, 2023
Accepted: July 13, 2023
Published: August 7, 2023

REFERENCES

1. Society of Automotive Engineers International (2016). Taxonomy and Definitions for Terms Related to Driving Automation Systems for On-Road Motor Vehicles (J3016_202104). latest revision 2021-04-30.

2. Talebpour, A., and Mahmassani, H.S. (2016). Influence of connected and autonomous vehicles on traffic flow stability and throughput. Transport. Res. C Emerg. Technol. *71*, 143–163. https://doi.org/10.1016/j.trc.2016.07.007.

3. Ye, L., and Yamamoto, T. (2019). Evaluating the impact of connected and autonomous vehicles on traffic safety. Phys. Stat. Mech. Appl. *526*, 121009. https://doi.org/10.1016/j.physa.2019.04.245.

4. Stern, R.E., Cui, S., Delle Monache, M.L., Bhadani, R., Bunting, M., Churchill, M., Hamilton, N., Haulcy, R., Pohlmann, H., Wu, F., et al. (2018). Dissipation of stop-and-go waves via control of autonomous vehicles: Field experiments. Transport. Res. C Emerg. Technol. *89*, 205–221. https://doi.org/10.1016/j.trc.2018.02.005.

5. Duan, X., Schockenhoff, F., and Koch, A. (2022). Implementation of driving cycles based on driving style characteristics of autonomous vehicles. World Electr. Veh. J. *13*, 108. https://doi.org/10.3390/wevj13060108.

6. Schoettle, B. (2017). Sensor Fusion: A Comparison of Sensing Capabilities of Human Drivers and Highly Automated Vehicles (The University of Michigan Sustainable Worldwide Transportation). Tech. rep.

7. Remonda, A., Veas, E., and Luzhnica, G. (2021). Comparing driving behavior of humans and autonomous driving in a professional racing simulator. PLoS One *16*, e0245320. https://doi.org/10.1371/journal.pone.0245320.

8. Kopelias, P., Demiridi, E., Vogiatzis, K., Skabardonis, A., and Zafiropoulou, V. (2020). Connected & autonomous vehicles – environmental impacts – a review. Sci. Total Environ. *712*, 135237. https://doi.org/10.1016/j.scitotenv.2019.135237.

9. Cui, D., Wang, Z., Liu, P., Wang, S., Zhang, Z., Dorrell, D.G., and Li, X. (2022). Battery electric vehicle usage pattern analysis driven by massive real-world data. Energy *250*, 123837. https://doi.org/10.1016/j.energy.2022.123837.

10. Weldon, P., Morrissey, P., Brady, J., and O'Mahony, M. (2016). An investigation into usage patterns of electric vehicles in ireland. Transport. Res. Transport Environ. *43*, 207–225. https://doi.org/10.1016/j.trd.2015.12.013.

11. Zhang, X., Zou, Y., Fan, J., and Guo, H. (2019). Usage pattern analysis of beijing private electric vehicles based on real-world data. Energy *167*, 1074–1085. https://doi.org/10.1016/j.energy.2018.11.005.

12. Cost, H., Braithwaite, J., Davis, P., Butler, P., Dowgiallo, E., Luca, W.D., Dzieciuch, M., Doddapaneni, N., Eskra, M., Freese, J., et al. (1996). Electric Vehicle Battery Test Procedures Manual (United States Advanced Battery Consortium). Tech. rep.

13. United States Environmental Protection Agency (2021). Dynamometer Drive Schedules.

14. André, M. (2004). The ARTEMIS European driving cycles for measuring car pollutant emissions. Sci. Total Environ. *334–335*, 73–84. Highway and Urban Pollution. https://doi.org/10.1016/j.scitotenv.2004.04.070.

15. Shim, B.J., Park, K.S., Koo, J.M., and Jin, S.H. (2014). Work and speed based engine operation condition analysis for new European driving cycle (NEDC). J. Mech. Sci. Technol. *28*, 755–761. https://doi.org/10.1007/s12206-013-1182-8.

16. Wipke, K., Cuddy, M., and Burch, S. (1999). ADVISOR 2.1: a user-friendly advanced powertrain simulation using a combined backward/forward approach. IEEE Trans. Veh. Technol. *48*, 1751–1761. https://doi.org/10.1109/25.806767.

17. Dettù, F., Pozzato, G., Rizzo, D.M., and Onori, S. (2021). Exergy-based modeling framework for hybrid and electric ground vehicles. Appl. Energy *300*, 117320. https://doi.org/10.1016/j.apenergy.2021.117320.

18. Sun, Z., Wen, Z., Zhao, X., Yang, Y., and Li, S. (2020). Real-world driving cycles adaptability of electric vehicles. World Electr. Veh. J. *11*, 19. https://doi.org/10.3390/wevj11010019.

19. Gong, H., Zou, Y., Yang, Q., Fan, J., Sun, F., and Goehlich, D. (2018). Generation of a driving cycle for battery electric vehicles: A case study of Beijing. Energy *150*, 901–912. https://doi.org/10.1016/j.energy.2018.02.092.

20. Baure, G., and Dubarry, M. (2019). Synthetic vs. real driving cycles: A comparison of electric vehicle battery degradation. Batteries *5*, 42. https://doi.org/10.3390/batteries5020042.

21. Oh, G., Leblanc, D.J., and Peng, H. (2022). Vehicle Energy Dataset (VED), a large-scale dataset for vehicle energy consumption research. IEEE trans. Intell. Transp. Syst. *23*, 3302–3312. https://doi.org/10.1109/TITS.2020.3035596.

22. Dembski, N., Guezennec, Y., and Soliman, A. (2002). Analysis and experimental refinement of real-world driving cycles. SAE Trans. *111*, 322–333. https://doi.org/10.4271/2002-01-0069.

23. Spagnol, P., Onori, S., Madella, N., Guezennec, Y., and Neal, J. (2010). Aging and characterization of Li-ion batteries in a HEV application for lifetime estimation. IFAC Proc. Vol. *43*, 186–191. 6th IFAC Symposium on Advances in Automotive Control. https://doi.org/10.3182/20100712-3-DE-2013.00186.

24. Liu, Z., Ivanco, A., and Onori, S. (2019). Aging characterization and modeling of nickel-manganese-cobalt lithium-ion batteries for 48V mild hybrid electric vehicle applications. J. Energy Storage *21*, 519–527. https://doi.org/10.1016/j.est.2018.11.016.

25. Shi, S., Zhang, M., Lin, N., and Yue, B. (2020). Low-cost reconstruction of typical driving cycles based on empirical information and low-frequency speed data. IEEE Trans. Veh. Technol. *69*, 8221–8231. https://doi.org/10.1109/TVT.2020.2997914.

26. M. Keefe, A. Simpson, K. Kelly, D. Pedersen, Duty Cycle Characterization and Evaluation towards Heavy Hybrid Vehicle Applications, SAE Technical Paper 2007-01-0302. https://doi.org/10.4271/2007-01-0302.

27. Rosewater, D., and Ferreira, S. (2016). Development of a frequency regulation duty-cycle for standardized energy storage performance testing. J. Energy Storage *7*, 286–294. https://doi.org/10.1016/j.est.2016.04.004.

28. Schoenwald, D.A., and Ellison, J. (2016). Determination of Duty Cycle for Energy Storage Systems in a PV Smoothing Application. Tech. rep. (Sandia National Laboratories). https://doi.org/10.2172/1331494.

29. Kucevic, D., Tepe, B., Englberger, S., Parlikar, A., Mühlbauer, M., Bohlen, O., Jossen, A., and Hesse, H. (2020). Standard battery energy storage system profiles: Analysis of various applications for stationary energy storage systems using a holistic simulation framework. J. Energy Storage *28*, 101077. https://doi.org/10.1016/j.est.2019.101077.

30. Moy, K., Lee, S.B., Harris, S., and Onori, S. (2021). Design and validation of synthetic duty cycles for grid energy storage dispatch using lithium-ion batteries. Adv. Appl. Energy *4*, 100065. https://doi.org/10.1016/j.adapen.2021.100065.

31. Ohzuku, T., Iwakoshi, Y., and Sawai, K. (1993). Formation of lithium-graphite intercalation compounds in nonaqueous electrolytes and their application as a negative electrode for a lithium ion (shuttlecock) cell. J. Electrochem. Soc. *140*, 2490–2498. https://doi.org/10.1149/1.2220849.

32. Harris, S.J., and Noack, M.M. (2023). Statistical and machine learning-based durability-testing strategies for energy storage. Joule *7*, 920–934. https://doi.org/10.1016/j.joule.2023.03.008.

33. Baumhöfer, T., Brühl, M., Rothgang, S., and Sauer, D.U. (2014). Production caused variation in capacity aging trend and correlation to initial cell performance. J. Power Sources *247*, 332–338. https://doi.org/10.1016/j.jpowsour.2013.08.108.

34. Hussain, A., and Rutgers, V. (2019). Change Is in the Air. Tech. rep. (Deloitte).

35. Yang, X.-G., Liu, T., Ge, S., Rountree, E., and Wang, C.-Y. (2021). Challenges and key requirements of batteries for electric vertical takeoff and landing aircraft. Joule *5*, 1644–1659. https://doi.org/10.1016/j.joule.2021.05.001.